AIAA JOURNAL
Vol. 34, No. 10, October 1996

Chemical Nonequilibrium Inviscid Flow over a Blunt Cone at Incidence

M. N. Macrossan* and C. Eckett†
University of Queensland, St. Lucia, Queensland 4072, Australia

Using a finite volume computational technique, we have investigated the chemically reacting inviscid flow of pure nitrogen over a blunt cone (half angle 13.5 deg) at an incidence of 30 deg. Although the effects of viscosity have been disregarded, the flow is three dimensional and contains a complex shock-vortical structure on the leeward surface of the blunt cone. We selected constant freestream conditions to correspond to those typical of the test section of ground based experimental facilities capable of producing strong dissociation effects. A range of cone sizes has been studied to produce flows ranging across the non-equilibrium regime as well as the limiting cases of chemically frozen (perfect gas) flow and flow that is in chemical equilibrium throughout. We found that the pitching moment coefficient on the body is a strong function of the degree of bluntness and that there are small but significant chemical effects superimposed on the bluntness effects. The effect of chemistry is most complicated for the bluntest body. There are strong chemical effects on the leeward flow.

Nomenclature

A_x	= base area of blunted cone of axial length x
C_z	= pitching moment coefficient, $M_z/(\frac{1}{2}\rho_\infty u_\infty^2 x A_x)$
$C_{z,\Delta}$	= C_z computed on grid with characteristic cell size Δ
e	= Richardson estimated error for a grid-dependent solution; Eq. (7)
H_0	= stagnation enthalpy
L_{chem}	= characteristic chemical length
M	= Mach number
M_z	= pitching moment about tip of blunt nose
$M_{z,l}$	= leeward pressure contribution to M_z
$M_{z,w}$	= windward pressure contribution to M_z
R	= gas constant for nitrogen
R_n	= blunt-nose radius
T	= temperature
u	= velocity
x	= axial length of blunt cone
α	= mass fraction of dissociated nitrogen
Δ	= characteristic computational cell size
δ	= angle of attack to freestream velocity
ϵ	= estimated error for a grid-dependent solution; Eq. (9)
θ	= cone half-angle
θ_d	= dissociation temperature
ρ	= density

Subscripts

l	= contribution from leeward forces only
w	= contribution from windward forces only
∞	= freestream conditions

I. Introduction

COMPARISONS of chemical and flow time scales for the typical flight trajectories of hypersonic aerospace planes and atmospheric re-entry vehicles indicate the aerothermodynamic conditions that can be experienced.[1] These range from chemically frozen flow, through a regime of nonequilibrium between the dissociation and recombination reactions, to equilibrium flow where local chemical equilibrium can be achieved within each fluid particle in times much smaller than the time it takes the fluid to traverse the vehicle.

Received Jan. 12, 1995; revision received April 11, 1996; accepted for publication April 18, 1996.

*Lecturer, Department of Mechanical Engineering. Member AIAA.
†Research Assistant, Department of Mechanical Engineering; currently Graduate Student, Graduate Aeronautical Laboratory 205-45, California Institute of Technology, Pasadena, CA 91125.

Stalker[1] presented a simplified analytical study of chemically reacting flow on the windward side of a blunt-nose flat plate at an angle of attack to show the importance of the rapid quenching[2] of the chemical reactions immediately behind the curved bow shock; there is a significant change in the pressure distribution downstream of the blunt nose, which leads to an increase of the nose-up pitching moment above the values experienced in the equilibrium or frozen chemistry limits.

Previous numerical studies of the hypervelocity, chemically reacting flow of a diatomic gas about a plane two-dimensional blunt-nose body[3] and about a sharp cone at an angle of attack[4] have supported Stalker's approximate analysis of the effects of reaction quenching behind the bow shock. In addition, the cone flow work[4] considered the chemical effects on the leeward flow, which contains a complex shock/vortical structure (see Sec. IV). By considering, among other things, the contributions made to the pitching moment by the windward and leeward pressure forces separately, Macrossan and Pullin[4] showed that the chemical effects were more complicated for the leeward flow and extended over a greater range of nonequilibrium.

The present computational work builds on the previous work by considering the effects of nose bluntness as well as chemical nonequilibrium. We have followed the procedure in the previous work of separating the integrated body forces, here in the form of pitching moment coefficients, into contributions from the windward and leeward forces. We show that the bluntness effects and the chemical rate effects in the nonequilibrium regime are different for the windward and leeward flows. We believe this is not only interesting in itself because of the different nature of the windward and leeward flows but also that it is useful to experimentalists working in short-duration, high-enthalpy wind tunnels to know the separate contributions that the windward and leeward forces make to the pitching moment. This is because it is possible that the windward flow, but not the leeward flow, will reach steady state within the short duration of the test flow.

The computational fluid dynamics method used is the equilibrium flux method.[5–8] For simplicity, the test gas is pure nitrogen so that the only chemical reactions are the dissociation reactions

$$N_2 + N \Leftrightarrow 2N + N \tag{1}$$

and

$$N_2 + N_2 \Leftrightarrow 2N + N_2 \tag{2}$$

These reactions and the similar reactions for the dissociation of O_2 are important for the aerodynamics of high-speed flight at near orbital speeds in the Earth's atmosphere. We use Lighthill's ideal dissociating gas model[9] with the appropriate chemical reaction rate equation[10] to represent the chemical dynamics of nitrogen, with experimental values of the reaction rate parameters.[11]

Table 1 Freestream conditions

Velocity u_∞, km s^{-1}	6.696
Density ρ_∞, 10^{-3} kg m^{-3}	9.974
Temperature T_∞, K	4469.0
Dissociation[a] α_∞	0.0113
Stagnation enthalpy H_0, MJ kg^{-1}	28.12
$H_0/(R\theta_d)$	0.83
Mach number[b] M_∞	5.000
Chemical length[c] L_{chem}, m	0.0032

[a] Value is at chemical equilibrium.
[b] Based on the frozen speed of sound.
[c] Reaction length behind a normal shock; see Eq. (3).

II. Freestream Conditions, Body Geometry, and Reaction Parameter

The freestream conditions are shown in Table 1 and are typical of a ground-based high-enthalpy test facility, a free piston driven shock tube wind tunnel. The stagnation enthalpy is 83% of the dissociation energy $R\theta_d$, which is sufficient to cause significant dissociation behind a strong shock. The freestream conditions differ from flight conditions at the same stagnation enthalpy in that the freestream temperature is higher and thus the Mach number is lower. There are some Mach number effects,[3] but these are generally smaller than the chemical effects.

The body was a blunted cone with a cone half-angle of $\theta = 13.5$ deg at an angle of attack to the freestream velocity of $\delta = 30$ deg. The blunt nose was spherical and its tangent (where it met the conical afterbody) was at an angle of 15 deg to the axis of the cone; thus there was a slight discontinuity at this point, the effect of which was assessed by repeating a typical calculation on a new grid with the discontinuity removed. Changes in the computed flow were negligible; for example, the drag coefficient changed by less than 0.02%.

A measure of the characteristic length introduced into the flow by the chemistry is given by the reaction length

$$L_{\text{chem}} = \frac{u_\infty}{(\mathrm{d}\alpha/\mathrm{d}t)_s} \tag{3}$$

where $(\mathrm{d}\alpha/\mathrm{d}t)_s$ is the dissociation rate evaluated for the density, temperature, and composition behind a normal shock (with the chemical reaction frozen across it); the value of L_{chem} is given in Table 1. We use the ratio of a characteristic body dimension to the chemical length as a reaction rate parameter.[11] It may also be expressed as the ratio of the fluid transit time past the body and the characteristic time required to effect the reaction; it is zero in the limit of frozen chemistry and infinite for a flow that is everywhere in local chemical equilibrium.

Although the conditions behind a normal bow shock might be expected to be characteristic of the flow near the blunt nose, they might not give the best characterization of the flow far downstream of the nose. In previous studies of the flow about a sharp cone,[4] the chemical length was calculated from conditions behind an oblique shock that was assumed coincident with the windward cone surface. This difference in definition of L_{chem} for sharp and blunt cones must be remembered when we refer to those previous results.

III. Grid Geometry and Computation Details

A. Description of Grid

The origin of Cartesian axes was placed at the tip of the blunt cone and the x axis coincided with the axis of the cone. The freestream velocity vector was parallel to the x–y plane, and because of the flow symmetry, only half of the flow ($z > 0$) was considered. A body-fitted grid of $N_1 \times N_2 \times N_3$ cells was used, where N_1 was the number of cells along the body in the axial direction, N_2 was the number normal to the body surface, and N_3 was the number between the windward and leeward planes of symmetry in the azimuthal direction. The cells were concentrated near the body surface and near the leeward plane of symmetry. In the axial (or N_1) direction, 20 cells were used from the tip to the end of the spherical nose and 60 more cells were used along the conical afterbody, which extended to a distance $x = 15R_n$; the cell sizes along the conical afterbody varied to keep the cell width an approximately constant fraction (0.09) of the local cone radius.

The calculation was performed in two stages. An initial calculation was performed on a subgrid of $N_1 \times N_2 \times N_3 = 27 \times 24 \times 50$, which extended seven cells past the spherical nose; in this nose subgrid, the governing equations were integrated forward in time from impulsive initial conditions until steady state was reached. The downstream conditions from the nose subgrid became the upstream boundary conditions for the remaining (afterbody) portion of the grid in which a space-marching technique was used; that is, steady state was found on successive slices, or subgrids, of size $N_1 \times N_2 \times N_3 = 3 \times 48 \times 100$, using the upstream boundary conditions found previously and a zero-gradient downstream boundary condition. After steady state was found in a subgrid, the conditions in the first upstream slice of the subgrid were saved to become upstream conditions for the next subgrid calculation, and the computational subgrid was moved downstream by one cell width and the process repeated. Space marching can only be successful if the flow is everywhere supersonic, and it is best if the gradients in the marching direction are small, as is true downstream of the nose in the flow considered here. Results for cone lengths $<15R_n$ (and hence blunter cones) were obtained from the same grid truncated at different lengths downstream, that is for a smaller number of computational cells overall.

An unsteady first-order Euler time-stepping method was used to find steady-state conditions. The ratio of the time step Δt to the smallest fluid or wave transit time across any cell was 0.5. Steady state was assumed when, for both energy and momentum, the net flux into every cell was reduced to less than 0.2% of the maximum flux across any of the six faces of the cell. In over 95% of the cells the net (residual) flux of both momentum and energy into the cell was much smaller than the maximum value of 0.2%, which occurred in a few cells near the stagnation point and near the windward bow shock.

A loose coupling approach to the calculation of the chemical reactions was taken in which the chemistry and fluid flux calculations were decoupled over the time interval Δt. At the end of each flux calculation (during which the chemical composition was frozen), the chemical reactions were advanced independently in each cell over the time Δt in an adiabatic process.[6] For chemically active flow, the total time-marching and space-marching calculation required a CPU time between 10 and 14 h on a Cray Y-MP/2D-216 computer.

B. Computational Accuracy

The cell sizes in the grid described in Sec. III.A, which was used as the production run grid, are essentially the same as those used for a sharp cone in earlier work[4] where it was determined that the grid was adequate by comparing the perfect gas (frozen chemistry) solution to that found with a more accurate shock-fitting, conical-flow method using a more refined grid.[12] Here we make a qualitative assessment of the errors in the computed pitching moment coefficient, C_z, the behavior of which is used later (see Secs. V.A and V.B) to characterize the nonequilibrium effects in the flow; we consider a nose radius of $R_n = 0.93L_{\text{chem}}$ for which nonequilibrium effects are maximum. We followed the procedure used by Blottner[13] and Walker and Oberkampf[14] and refined the grid independently in each direction. It was not possible, because of the available computational power, to perform calculations on grids with twice the number of cells in any direction, and so we used grids constructed by halving, and halving again, the number of cells in each grid direction. Thus the following three series of grids were used for the three independent grid refinement studies:

N_1 varies: $(20 \times 48 \times 104)$, $(40 \times 48 \times 104)$, $(80 \times 48 \times 104)$

N_2 varies: $(80 \times 12 \times 104)$, $(80 \times 24 \times 104)$, $(80 \times 48 \times 104)$

N_3 varies: $(80 \times 48 \times 26)$, $(80 \times 48 \times 52)$, $(80 \times 48 \times 104)$

Note that N_1 is the sum of the numbers of axial cells in the nose and afterbody subgrids, whereas N_2 and N_3 refer to the numbers of cells in the afterbody subgrid (the nose subgrid has half the preceding numbers of cells in the N_2 and N_3 directions). The most refined grid,

which was the same in each series ($80 \times 48 \times 104$), was slightly finer than the ($80 \times 48 \times 100$) production grid, but because of the two-stage calculation method that started on the less fine nose subgrid, it was necessary that the largest value of N_3 in the afterbody subgrid be divisible by 8. In view of the very small change in the computed value of C_z between the fine and medium grids [<0.4%; see Eq. (9)], it is reasonable to assume that the estimated relative errors for the grid with $N_3 = 104$ are a very good estimate of the errors associated with the production grid for which $N_3 = 100$.

We expect the computed estimate of the pitching moment coefficient $C_{z,\Delta}$ to be related to the exact value $C_{z,0}$ by

$$C_{z,\Delta} = C_{z,0} + b_1\Delta^{p_1} + b_2\Delta^{p_2} + b_3\Delta^{p_3} + \cdots \text{(higher-order terms)} \quad (4)$$

where b_j and p_j are constants and Δ is 1, 2, and 4 for the fine, medium, and coarse grids, respectively. Note that Eq. (4) does not imply that the cell size is Δ in each direction, just that all cell sizes are fixed multiples of some (arbitrary) characteristic cell size as the grid is refined. When estimates of C_z are obtained on different grids that vary in the number of cells in one direction only, the computed value is expected to be given by

$$C_{z,\Delta} = C_{z,0} + b_j\Delta^{p_j} + \text{const} + \cdots \text{(higher-order terms)} \quad (5)$$

If the grid is sufficiently fine, the higher-order terms in Eq. (5) can be ignored and the exact value can be estimated by Richardson extrapolation as

$$C_{z,0} \approx \frac{2^{p_j}C_{z,1} - C_{z,2}}{2^{p_j} - 1} \quad (6)$$

The relative error in the fine grid solution, $C_{z,1}$, can be estimated as

$$e_j = \left|\frac{C_{z,1} - C_{z,0}}{C_{z,0}}\right| = \left|\frac{C_{z,1} - C_{z,2}}{2^{p_j}C_{z,1} - C_{z,2}}\right| \quad (7)$$

The computational method[7,8] uses the min-mod or MUSCL strategy[15] to reconstruct the flow properties at interfaces between cells before calculating the fluxes. In most of the flow, piecewise linear gradients are used, and the method is nominally second order ($p = 2$) in those regions. However, in cells in which there is a local maximum or minimum of a flow property in a coordinate direction, a piecewise constant (no gradient) reconstruction is used in that direction for that variable, and the method reverts to first-order accuracy ($p = 1$) locally. It was found for the N_1 and N_2 coordinate directions that $p = 2$ gave a good fit to the results on the three grids and that the best fit value of p was 1.5 for the body normal (N_2) direction; that is, the method is second order in the axial and azimuthal directions but of a lower order in the body normal direction. This lower-order accuracy in the body normal direction is to be expected because the bow shock is smeared across a few cells in that direction, and the method reverts to first-order accuracy, at least at the shock location.

The estimated errors as N_1 or N_2 or N_3 is varied are shown in Fig. 1. Since $N_j \propto 1/\Delta$, the error points for each convergence study lie on straight lines on this log e v log N_j plot with slopes of -2, -1.5, and -2. The errors for the finest grid solution for the three directions were $e_1 = 0.016\%$, $e_2 = 0.203\%$, and $e_3 = 0.045\%$, and the total error in the pitching moment coefficient can be estimated as the sum of these three values, 0.264%. Because the convergence rate for the mixed first- and second-order method cannot be determined formally, it is not possible to say with certainty that the asymptotic limit has been reached for the N_2 direction for which p_2 was estimated to be 1.5. It is because of such uncertainties (and others) that Roache[16] suggests the use of a conservative measure of the error, the grid convergence index (GCI), which is larger than the error estimated from Richardson's extrapolation. The grid convergence index is related to the error estimate of Eq. (7) by

$$GCI = 3\frac{2^{p_j} - (1+\epsilon)}{2^{p_j} - 1}e_j \quad (8)$$

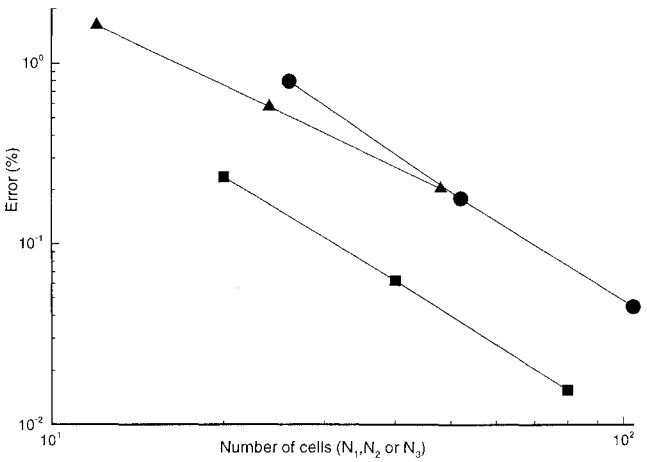

Fig. 1 Errors in calculated pitching moment on three series of grids with varying numbers of cells, estimated using Richardson extrapolation: ■ — N_1 varies, $N_2 = 48$, $N_3 = 104$, and $p = 2.0$; ▲ — N_2 varies, $N_1 = 80$, $N_3 = 104$, and $p = 1.5$; ● — N_3 varies, $N_1 = 80$, $N_2 = 48$, and $p = 2.0$; and $R_n/L_{\text{chem}} = 0.93$. Cone length $x = 10.9R_n$.

where

$$\epsilon = \left|\frac{C_{z,1} - C_{z,2}}{C_{z,1}}\right| \quad (9)$$

The values of ϵ, the fractional change in C_z between the fine and medium grids, were all less than 0.4%, for which Eq. (8) reduces to $GCI \approx 3e_j$. Following Roache,[16] an upper estimate of the error in the fine grid (and production run grid) solution for the pitching moment coefficient would be $3 \times 0.263\% \approx 0.8\%$. Identical analyses for the cases of frozen and equilibrium chemistry showed GCI errors of 0.32 and 1.07%, respectively.

The following work describes some small changes in the pitching moment coefficient (on the order of 2%) that are not a great deal larger than the grid error of $\approx 1\%$ reported here. However, the grid error is systematic, not random; for the three cases of frozen chemistry, maximum nonequilibrium chemistry, and equilibrium chemistry, the numerical computation yields a value of C_z that is less than the extrapolated exact value. Thus the trends observed in the reported numerical results would be expected to be seen in any set of theoretically exact (grid-independent) data.

IV. Blunt Cone Flow

The general nature of the nonequilibrium flow is shown in Fig. 2, which shows Mach number contours for the case when the nose radius R_n was comparable in magnitude to the chemical length L_{chem}. The contours in the windward and leeward plane of symmetry show the highly curved bow shock ahead of the blunt nose. Away from the blunt nose, the bow shock becomes an approximately conical shock that is strong and close to the body on the windward side and weak and diffuse on the leeward side. The contours on the windward plane of symmetry also show a secondary or embedded leeward shock behind the bow shock. This embedded shock begins near the cone surface where the spherical nose meets the conical afterbody and can be expected to arise whenever there is a discontinuity in curvature in the body surface[17]; it would be weakened somewhat by the discontinuity in tangent where the spherical nose meets the afterbody, from which a weak expansion fan should propagate.

The contours on the cross section at the rear of the body show the shock-vortical structure that develops in the flow near the leeward body surface. This arises because the flow that crosses the bow shock near the windward plane of symmetry, but somewhat downstream of the blunt nose, expands around the cone surface, becoming supersonic before going through a crossflow shock that turns the flow approximately parallel to the leeward plane of symmetry. The structure of this leeward flow for a sharp cone was shown in detail by Marconi[12] for a perfect gas (chemically frozen) flow and for a reacting flow by Macrossan and Pullin.[4] The results shown in

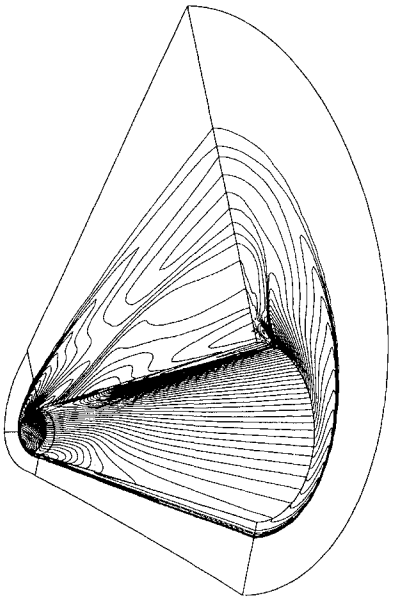

Fig. 2 Contours of Mach number M for $R_n/L_{\text{chem}} = 3.1$. Contours are shown on the body surface, the windward and leeward planes of symmetry, and a surface roughly normal to the rear surface of the body.

Fig. 2 indicate that the flow at the rear of the body is roughly similar to the flow seen about a sharp cone; the results shown in Sec. V.A give another indication that the flow is reasonably close to conical at this distance of approximately $14R_n$ from the blunt nose.

Figure 3 shows the temperature contours in a cross section of the flow at $x/R_n = 4$, for a range of cone sizes ($0.31 \leq R_n/L_{\text{chem}} \leq 310$) that spans the regime of nonequilibrium flow. As was seen for the flow over a sharp cone,[4] the closely spaced contours in the radial direction behind the windward shock represent a region of dissociation cooling where the dissociation reaction rate is quickly quenched as described by Hornung.[18] For atmospheric freestream conditions the quenched state would be far removed from equilibrium, but for the shock tunnel freestream conditions used here, for which the density is greater, it is possible for local equilibrium to be reached before the flow expands towards the leeward side of the body.[3,4] The dissociation cooling region extends from the shock to the body near the windward plane of symmetry for $R_n/L_{\text{chem}} = 0.31$ and 3.1. As R_n/L_{chem} increases, that is, as the reaction length becomes smaller relative to the body size, the rapid cooling region contracts towards the shock as expected. The flow in the shock layer also goes through a region of cooling as it expands towards the leeward side of the body. The spacing of the temperature contours in the azimuthal direction shows that the expansion cooling is less severe than the dissociation cooling behind the shock.

The flow patterns at the same cross section are shown in Fig. 4 for the limiting cases of frozen and equilibrium chemistry. They are similar to each other, except that the temperature gradient is smaller in the equilibrium flow because of the exothermic recombination reaction that takes place through the expansion. The frozen chemistry and equilibrium chemistry flows are quite different from the chemically nonequilibrium flows shown in Fig. 3. For example, there is no quenching region, for obvious reasons in the case of frozen chemistry, and because the dissociation takes place within the shock rather than following it in the case of equilibrium chemistry; there is also a thermal heating layer near the body surface where the high-temperature fluid that crossed the bow shock near the stagnation point expands around the body close to the surface. This thermal layer is present to a much lesser degree in the nonequilibrium flows of Figs. 3c and 3d and is absent from those in Figs. 3a and 3b, where the quenching effect reverses the direction of the temperature gradient adjacent to the body surface.

Bluntness effects may be examined in Fig. 5, which shows temperature contours at a range of downstream stations along a body for which $R_n/L_{\text{chem}} = 3.1$. As will be seen in Secs. V.A and V.B, this is close to the body size for which nonequilibrium effects are

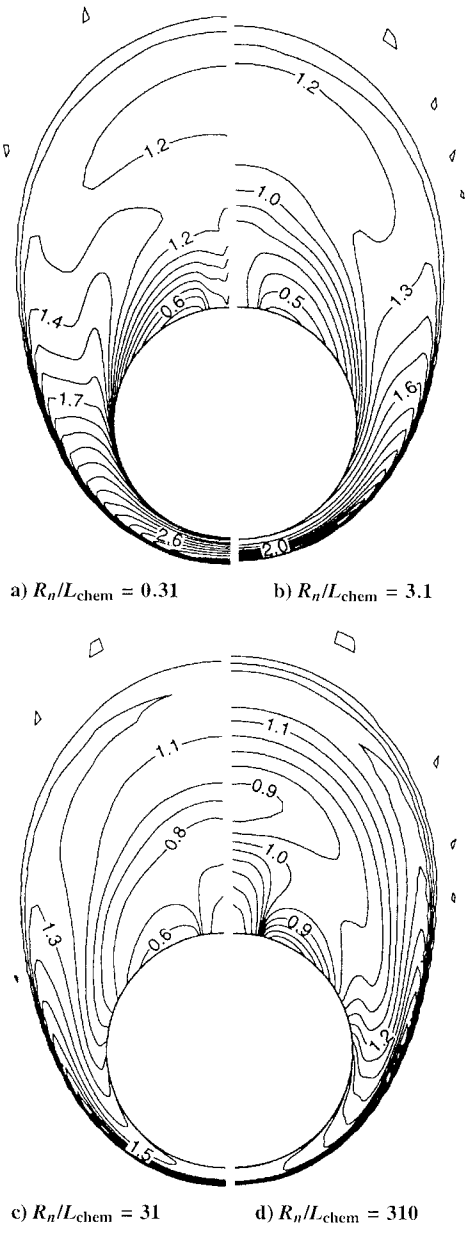

a) $R_n/L_{\text{chem}} = 0.31$ b) $R_n/L_{\text{chem}} = 3.1$

c) $R_n/L_{\text{chem}} = 31$ d) $R_n/L_{\text{chem}} = 310$

Fig. 3 Contours of temperature T/T_∞ in a cross-section of the flow at $x/R_n = 4$.

greatest. On the windward side, the flow patterns are similar for all values of the normalized axial cone length x/R_n, but the flow on the leeward side depends strongly on x/R_n. The crossflow shock and vortex structure characteristic of flow over sharp cones at angles of attack[4,12] does not develop until somewhere between 4 and 7 nose radii downstream of the nose tip.

V. Integrated Body Forces

We consider the pitching moment about the z axis through the tip of the nose, divided into separate contributions from the windward and leeward pressure forces. Thus,

$$M_z = M_{z,w} + M_{z,l} \tag{10}$$

where

$$M_{z,w} = \int_{\boldsymbol{u}_\infty \cdot \hat{\boldsymbol{n}} < 0} p_s \hat{\boldsymbol{k}} \cdot \hat{\boldsymbol{n}} \times \boldsymbol{r}_s \, \mathrm{d}A_s \tag{11}$$

$$M_{z,l} = \int_{\boldsymbol{u}_\infty \cdot \hat{\boldsymbol{n}} > 0} p_s \hat{\boldsymbol{k}} \cdot \hat{\boldsymbol{n}} \times \boldsymbol{r}_s \, \mathrm{d}A_s \tag{12}$$

and where $\hat{\boldsymbol{n}}$ is the outward-pointing unit vector normal to an element of the body surface $\mathrm{d}A_s$, p_s is the pressure acting on that element,

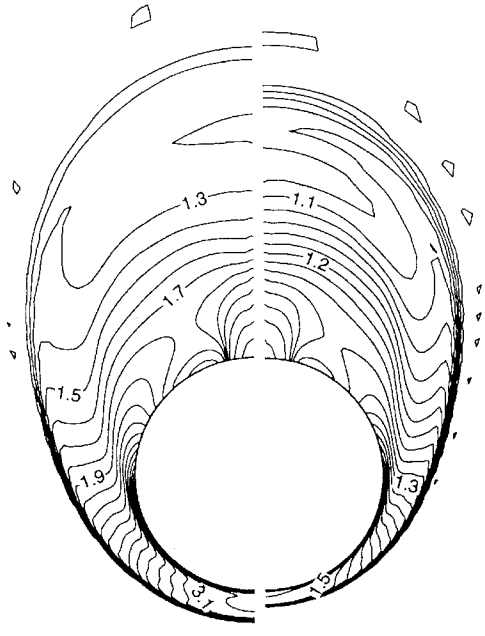

a) Frozen chemistry b) Equilibrium chemistry

Fig. 4 Contours of temperature T/T_∞ in a cross section of the flow at $x/R_n = 4$.

$\mathbf{r}_s$ is the position vector from the tip of the nose to the element, and $\hat{\mathbf{k}}$ is the unit vector along the z axis. The base surface of the body is excluded from the integration as the flow calculations did not extend past the end of the conical body. The very last layer of cells in the streamwise direction, which would be most affected by errors introduced by the space-marching technique, was discarded. Thus the maximum body length for which a pitching moment was calculated was approximately $14.5R_n$. Results for smaller cone lengths were obtained by truncating the integration of Eqs. (11) and (12) at the desired distance x from the blunt nose.

We estimated the surface shear stresses on the blunt cone using the theory for compressible turbulent flow over a flat plate as summarized by Stollery.[19] At every element of the cone surface, the boundary-layer outer flow boundary conditions (pressure, temperature, and Mach number) were taken to be the same as the wall conditions found in our inviscid calculations. The wall stresses were then increased by a factor of $\sqrt{3}$ to account for the change from flat plate to a cone.[20] The resulting wall stresses were assumed to act in the direction of the wall slip velocity obtained from the inviscid calculations, and the approximate shear forces were integrated numerically over the entire cone surface. The shear stress contribution to the body force coefficients depends (through the Reynolds number) on the cone length, which was varied in the inviscid calculations. The maximum effects were found for a body size of ≈ 15 mm, which is a typical test section model size, and for a cold model wall. The shear stresses are small relative to the pressure; it was estimated that the shear forces could increase the drag by up to 4%. What is relevant to this work, however, is the possible effect of shear stresses on the moment coefficients compared with the effects of chemistry and nose bluntness; it was estimated that the windward component of the pitching moment could be increased by up to 0.7% and the leeward component of pitching moment could be increased by up to 1.5%.

A. Windward Contribution to Pitching Moment

Figure 6 shows the data for the windward pitching moment coefficient up to a distance x from the tip of the nose,

$$C_{z,w} = \frac{M_{z,w}}{\frac{1}{2}\rho_\infty u_\infty^2 x A_x} \tag{13}$$

where $M_{z,w}$ is given in Eq. (11). The first data point ($x/R_n \approx 0.77$) is for a body truncated immediately after the spherical nose. It will be seen later that the contribution to the total pitching moment from the leeward pressure forces is $\approx \frac{1}{10}$ of the contribution of the windward

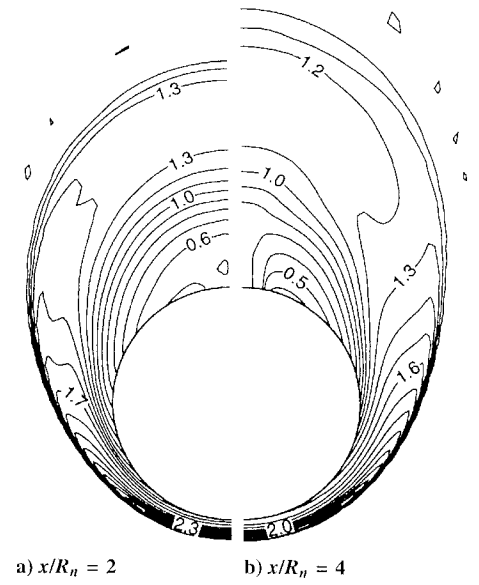

a) $x/R_n = 2$ b) $x/R_n = 4$

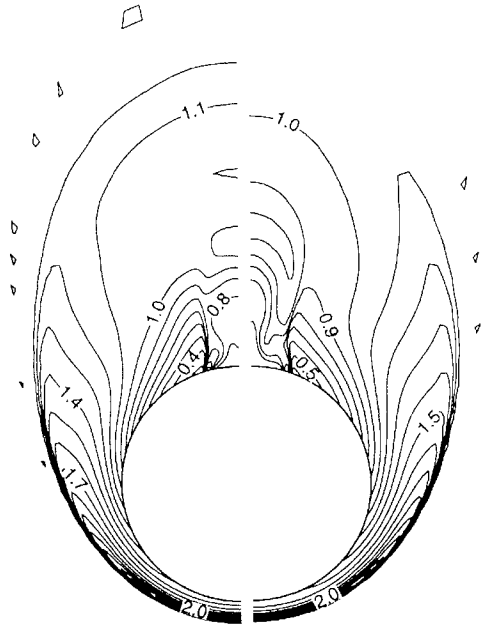

c) $x/R_n = 7$ d) $x/R_n = 12$

Fig. 5 Contours of temperature T/T_∞ at various cross sections of the flow for $R_n/L_{\text{chem}} = 3.1$ and normalized cone length.

forces considered here. Thus $C_{z,w}$ is very close to the pitching moment coefficient, which would be important for the aerodynamic stability of this blunt body.

It is evident from Fig. 6 that the effect of bluntness on $C_{z,w}$ is much greater than the effect of chemistry; the variation in $C_{z,w}$ over the range of normalized axial cone lengths x/R_n is approximately 35%. In all cases $C_{z,w}$ has a sharp minimum at $x/R_n \approx 1.3$, which is a very blunt cone consisting almost entirely of the spherical nose. For larger values of x/R_n the pitching moment increases, apparently approaching a limiting value as $x/R_n \to \infty$, as would be expected for a sharp cone, although that limiting value has not been reached at $x/R_n \approx 14$.

For all degrees of bluntness shown in Fig. 6, the effect of different values of the reaction rate parameter R_n/L_{chem} is at most 2%, but a change of 2% in the pitching moment for a flight vehicle with a fixed shape, traversing a range of different chemical conditions in its trajectory, can be significant.[1,21,22]

This chemical effect can be seen more clearly in Fig. 7, which shows data for the windward pitching moment as the reaction rate parameter R_n/L_{chem} varies from extremely small (frozen chemistry) to very large (equilibrium chemistry). Results are shown for

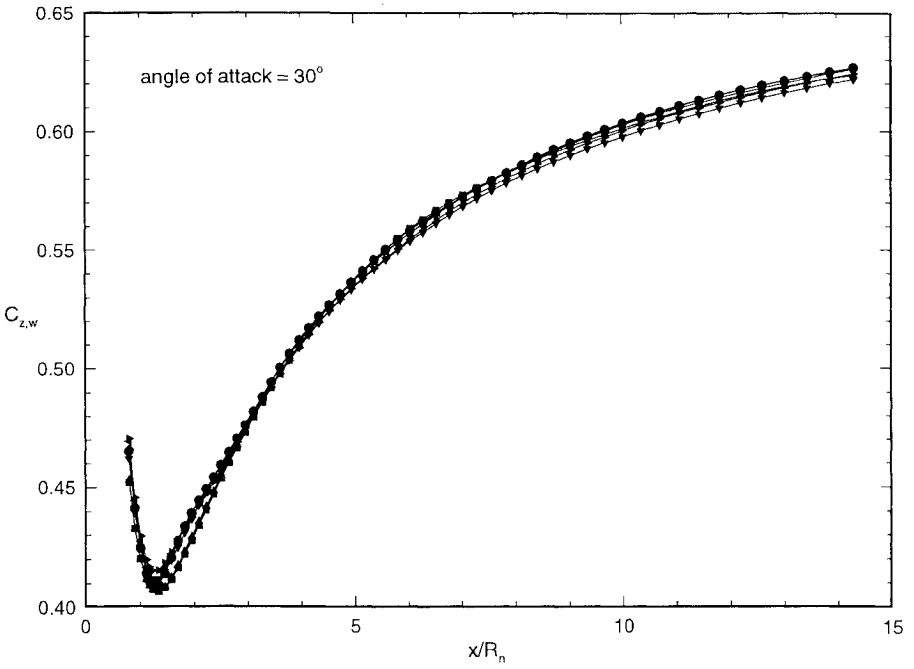

Fig. 6 Windward pitching moment coefficient $C_{z,w}$ vs normalized axial cone length x/R_n for a range of reaction rate parameters R_n/L_{chem}; integrated pitching moment of windward pressure forces up to the distance x: ■, frozen chemistry; ▲, $R_n/L_{chem} = 0.031$; ▼, $R_n/L_{chem} = 0.31$; ►, $R_n/L_{chem} = 9.3$; ◄, $R_n/L_{chem} = 93$; ♦, $R_n/L_{chem} = 930$; and •, equilibrium chemistry.

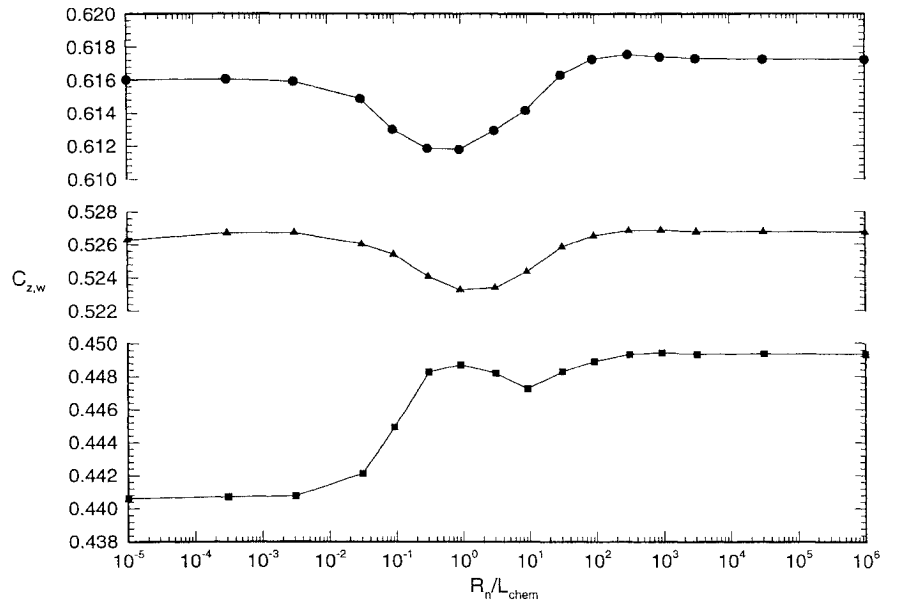

Fig. 7 Windward pitching moment coefficient $C_{z,w}$ vs reaction rate parameter R_n/L_{chem} for three values of normalized axial cone length x/R_n: ■, $x/R_n = 2.2$; ▲, $x/R_n = 4.5$; and •, $x/R_n = 12.2$.

three different body shapes, with normalized axial cone lengths of $x/R_n = 2.2, 4.5$, and 12.2. In each case the regime of chemical nonequilibrium is given approximately by $3 \times 10^{-3} \leq R_n/L_{chem} \leq 10^3$. The pitching moment for frozen chemistry flow is below that for chemical equilibrium flow.

The results for the longest ($x = 12.2R_n$) and hence the sharpest cone are very close to those found for a sharp cone[4] for the same freestream conditions and angle of attack and a cone half-angle very close to that in the present computations. In those cases and also for a shorter ($x = 4.5R_n$) and hence blunter cone, the values of moment for frozen and equilibrium chemistry are similar, whereas in the intermediate regime of nonequilibrium chemistry, where $R_n/L_{chem} = \mathcal{O}(1)$, $C_{z,w}$ does not always lie between the values found for frozen and equilibrium chemistry. If one looks at the curves starting from the limit of equilibrium chemistry and proceeding to the nonequilibrium regime one first sees similar behavior in all cases in that the pitching moment begins to decrease at $R_n/L_{chem} \approx 1000$. There is a local minimum in $C_{z,w}$ in the nonequilibrium regime; the reduction in $C_{z,w}$ is about 1% for the sharper cones and somewhat less for the bluntest cone. The rise in $C_{z,w}$ after the local minimum is monotonic towards the value for frozen chemistry for the sharpest cone, whereas for the blunter cones the initial rise is followed by a fall that is slight for the moderately blunted cone, $x/R_n = 4.5$, but much greater for $x/R_n = 2.2$. In the last case, the value of $C_{z,w}$ for frozen chemistry is some 2% less than the value for equilibrium chemistry.

Figure 7 demonstrates that the transition from the limit of frozen chemistry to the chemical equilibrium limit is not a simple one and

that consideration of the limiting cases may not be sufficient for design purposes. This was suggested by the simplified analytical model of Stalker[1] and supported by the numerical results for a blunted flat plate[3] and for a sharp cone[4]; it has been shown here that it holds for the more realistic blunted cone shape and that the extent of departure from nonequilibrium flow depends on the degree of bluntness of the body. For very blunt cones, an assumed design value of $C_{z,w}$ that remained within the limits set by equilibrium and frozen chemistry flow calculations would be reasonable; for moderately blunted and sharp cones it would not.

The variation of the windward pitching moment coefficient with chemical reaction rate is not a great deal larger than the 0.7% contribution that shear stresses may make to the windward pitching moment coefficient. The variation of shear stresses for different chemical reaction rates is unknown; therefore the chemical effect on the pitching moment derived from the pressure forces only must be treated with some caution. However, it is probable that the shear stresses are no more sensitive to reaction rate than are the pressure forces. If so, then a small variation in the distribution of the shear stresses will make only a negligibly small change in the already very small contribution that shear stresses make to the pitching moment coefficient.

B. Leeward Contribution to Pitching Moment

Although the leeward pressure makes a small contribution only to the aerodynamic forces acting on the body ($< 4\%$), it is nevertheless interesting to note the effect of chemistry on the complex shock-vortical structure in the leeward flow. Figure 8 shows the leeward component of the pitching moment coefficient up to a distance x from the tip of the nose given by

$$C_{z,l} = \frac{M_{z,l}}{\frac{1}{2}\rho_\infty u_\infty^2 x A_x} \tag{14}$$

where $M_{z,l}$ was determined from Eq. (12).

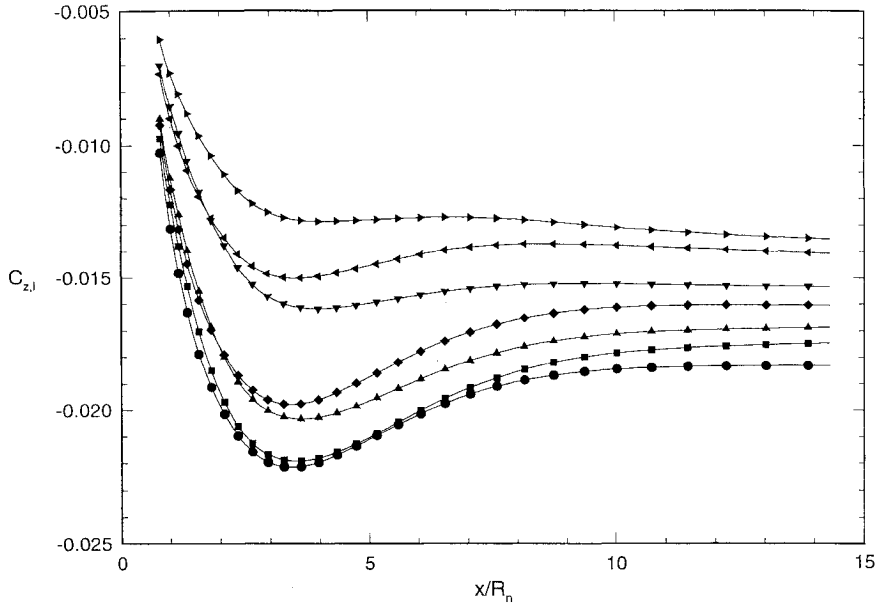

Fig. 8 Leeward pitching moment coefficient $C_{z,l}$ vs normalized axial cone length x/R_n for different values of reaction rate parameter R_n/L_{chem}; integrated moment of leeward pressure forces up to the distance x: ■, frozen chemistry; ▲, $R_n/L_{chem} = 0.031$; ▼, $R_n/L_{chem} = 0.31$; ►, $R_n/L_{chem} = 9.3$; ◄, $R_n/L_{chem} = 93$; ♦, $R_n/L_{chem} = 930$; and ●, equilibrium chemistry.

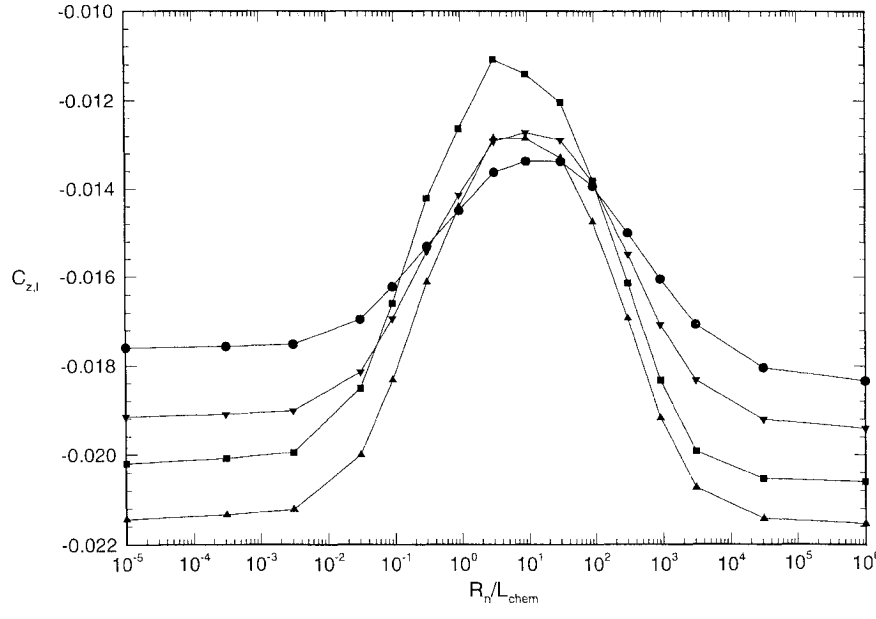

Fig. 9 Leeward pitching moment coefficient $C_{z,l}$ vs reaction rate parameter R_n/L_{chem} for four values of normalized axial cone length x/R_n: ■, $x/R_n = 2.2$; ▲, $x/R_n = 4.5$; ▼, $x/R_n = 7.0$; and ●, $x/R_n = 12.2$.

In contrast to the insensitivity of the windward pitching moment to the reaction rate parameter (see Fig. 6), the effect of chemistry on $C_{z,l}$ is approximately 25%. The effect of bluntness is also about 25%, somewhat less than the bluntness effect on the windward pitching moment. Both the bluntness and chemistry effects are much larger than the expected effect of shear stresses on the leeward flow ($\approx 1.5\%$). For the limiting cases of frozen and equilibrium chemistry, there is a local minimum in pitching moment coefficient before it rises to approach a limiting value for less blunt cones. This is similar to the behavior of the windward pitching moment for all values of reaction rate parameter, but here the minimum is farther from the nose, at $x/R_n \approx 4$, and the downstream limit seems to be reached by $x/R_n \approx 10$, whereas the limit had not been reached for the windward moment at $x/R_n \approx 14.5$. The local minimum in the curve is least severe for $R_n/L_{\text{chem}} = 9.3$, suggesting that bluntness effects are moderated around the range $R_n/L_{\text{chem}} = \mathcal{O}(1)$. Conversely, the bluntness effect is most pronounced for the cases of frozen chemistry and equilibrium chemistry.

Figure 9 shows data for $C_{z,l}$ plotted against the reaction rate parameter R_n/L_{chem} for different values of x/R_n. Unlike the case for the windward pitching moment (Fig. 7), the general trend is the same in all cases; the values for frozen and equilibrium chemistry differ by 1–4%, and there is large departure in the nonequilibrium regime of 40–50% for the low values of x/R_n (blunt cones) and about 20–30% for the high values of x/R_n (relatively sharp cones). The departure from the equilibrium chemistry limit occurs at $R_n/L_{\text{chem}} \approx 3 \times 10^4$, which is more than an order of magnitude higher than for the windward flow. The reaction rate at which the maximum deviation from the equilibrium value of $C_{z,l}$ occurs is given by $R_n/l_{\text{chem}} \approx 30$ for $x/R_n = 12.2$ and by $R_n/L_{\text{chem}} \approx 3$ for $x/R_n = 2.2$.

VI. Conclusions

In considering the effects of nose bluntness, this work has supplemented previous work on chemical rate effects on the flow about sharp cones at an angle of attack. In this and the previous work, the effects of viscosity on the flow have been omitted in the interests of studying the important effects of nonequilibrium chemistry on a relatively simple three-dimensional flow. It was found that the effect of a blunt nose is moderate at a distance of approximately $7R_n$ downstream of the blunt nose and is small at a distance of approximately $15R_n$ downstream (see Figs. 6 and 8). The flow patterns, as shown by the temperature contours in a plane normal to the cone axis, show the rapid quenching of the dissociation reactions behind the bow shock, which occurs (for a moderately blunt cone of length $x = 4R_n$) when the nose radius R_n is comparable in magnitude to the characteristic reaction length behind the bow shock.

The effects of bluntness on the windward and leeward part of the flow have been considered separately. The major contribution to the pitching moment comes from the pressure forces on the windward side of the cone and the pitching moment coefficient $C_{z,w}$ is a strong function of bluntness (see Fig. 6). The variation of $C_{z,w}$ with reaction rate parameter (which can be experienced in the varying conditions along a re-entry trajectory) is only a few percent, but this can be enough to have important effects on the aerodynamic stability of the blunt body. The variation is more complicated for the blunter cone than the sharper cone (see Fig. 7). The estimated magnitude of the surface shear stress contribution to the pitching moment is small compared with that from the pressure forces, and it might be expected that shear stresses could make no difference to the conclusions drawn here on the basis of the pressure forces only. If the shear stresses are much more sensitive to chemical nonequilibrium effects than are the pressure forces, these conclusions might have to be revised.

A complex shock-vortical structure develops on the leeward surface of a sharp cone and also on the moderately blunt cones considered here. Bluntness effects on the leeward flow for equilibrium and frozen chemistry conditions are less than for the windward flow and are reduced even further for values of the reaction rate parameter $\approx \mathcal{O}(1)$ (see Fig. 8). Chemistry effects are greater than on the windward side and extend over a greater range of reaction rate parameters. The leeward flow is likely to be determined by the conditions at the leeward crossflow shock rather than those immediately behind windward bow shock that were used to define the reaction rate parameter.

Acknowledgment

This work was supported by the Australian Research Council under Grant A89031403.

References

[1]Stalker, R. J., "Approximations for Non-Equilibrium Hypervelocity Aerodynamics," *AIAA Journal*, Vol. 27, No. 12, 1989, pp. 1761–1769.

[2]Hornung, H. G., "Experimental Real-Gas Hypersonics," *Aeronautical Journal*, Vol. 92, No. 920, 1988, pp. 379–389.

[3]Macrossan, M. N., "Hypervelocity Flow of Dissociating Nitrogen Downstream of a Blunt Nose," *Journal of Fluid Mechanics*, Vol. 217, Aug. 1990, pp. 167–202.

[4]Macrossan, M. N., and Pullin, D. I., "A Computational Investigation of Inviscid Hypervelocity Flow of a Dissociating Gas Past a Cone at Incidence," *Journal of Fluid Mechanics*, Vol. 266, May 1994, pp. 69–92.

[5]Pullin, D. I., "Direct Simulation Methods for Compressible Ideal Gas Flow," *Journal of Computational Physics*, Vol. 34, No. 2, 1980, pp. 231–244.

[6]Macrossan, M. N., "The Equilibrium Flux Method for the Calculation of Flows with Non-Equilibrium Chemical Reactions," *Journal of Computational Physics*, Vol. 80, No. 1, 1989, pp. 204–231.

[7]Macrossan, M. N., and Pullin, D. I., "Hypervelocity Cone-Flow with Reaction Chemistry by a Second Order Kinetic Theory Based Euler Solver," *3rd Australian Supercomputer Conference, University of Melbourne December 1990*, edited by K. Sweeney, Strategic Research Foundation, Univ. of Melbourne, Australia, 1990, Session 4.3.

[8]Mallett, E. R., Pullin, D. I., and Macrossan, M. N., "Numerical Study of Hypersonic Leeward Flow over a Blunt Nosed Delta Wing," *AIAA Journal*, Vol. 33, No. 9, 1995, pp. 1626–1633.

[9]Lighthill, M. J., "Dynamics of a Dissociating Gas. Part I. Equilibrium Flow," *Journal of Fluid Mechanics*, Vol. 2, Jan. 1957, pp. 1–32.

[10]Freeman, N. C., "Non-Equilibrium Flow of an Ideal Dissociating Gas," *Journal of Fluid Mechanics*, Vol. 4, Aug. 1958, pp. 407–425.

[11]Kewley, D. J., and Hornung, H. G., "Free-Piston Shock-Tube Study of Nitrogen Dissociation," *Chemical Physics Letters*, Vol. 25, No. 4, 1974, pp. 531–536.

[12]Marconi, F., "Complex Shock Patterns and Vortices in Inviscid Supersonic Flows," *Computer and Fluids Journal*, Vol. 17, No. 1, 1989, pp. 151–163.

[13]Blottner, F. G., "Accurate Navier–Stokes Results for the Hypersonic Flow over a Spherical Nosetip," *Journal of Spacecraft and Rockets*, Vol. 4, No. 2, 1990, pp. 113–122.

[14]Walker, M. A., and Oberkampf, W. L., "Joint Computational/Experimental Aerodynamics Research on a Hypersonic Vehicle, Part 2: Computational Results," *AIAA Journal*, Vol. 30, No. 8, 1992, pp. 2010–2016.

[15]Van Leer, B., "Towards the Ultimate Conservative Difference Scheme, Part V," *Journal of Computational Physics*, Vol. 32, No. 1, 1979, pp. 101–136.

[16]Roache, P. J., "Perspective: A Method for Uniform Reporting of Grid Refinement Studies," *Journal of Fluids Engineering*, Vol. 116, Sept. 1994, pp. 405–413.

[17]Rusanov, V. V., "A Blunt Body in a Supersonic Stream," *Annual Review of Fluid Mechanics*, Vol. 8, 1976, pp. 377–404.

[18]Hornung, H. G., "Non-Equilibrium Ideal Dissociation After a Curved Shock Wave," *Journal of Fluid Mechanics*, Vol. 74, March 1976, pp. 143–160.

[19]Stollery, J. L., "Supersonic Turbulent Boundary Layers: Some Comparisons Between Experiment and a Simple Theory," *Aeronautical Quarterly*, Vol. 27, May 1976, pp. 87–98.

[20]White, F. M., *Viscous Fluid Flow*, 2nd ed., McGraw–Hill, New York, 1991.

[21]Maus, J. R., Griffith, B. J., and Szema, K. Y., "Hypersonic Mach Number and Real Gas Effects on Space Shuttle Orbiter Aerodynamics," *Journal of Spacecraft and Rockets*, Vol. 21, No. 2, 1984, pp. 136–141.

[22]Griffith, B. J., Maus, J. K., Majors, B. M., and Best, J. T., "Addressing the Hypersonic Simulation Problem," *Journal of Spacecraft and Rockets*, Vol. 24, No. 4, 1987, pp. 334–341.